Chemical Science

ROYAL SOCIETY OF CHEMISTRY

EDGE ARTICLE

View Article Online
View Journal

Cite this: DOI: 10.1039/d5sc09108j

All publication charges for this article have been paid for by the Royal Society of Chemistry

Ultra-low concentration gel polymer electrolytes realize stable and low-temperature lithium–organic batteries

Mengjie Li,[ab] Hang Liu,[a] Hai Su,[a] Zehui Fan,[a] Yuansheng Liu,[a] Jixing Yang,*[a] Wei Zhu,[a] Qinghao Chen[a] and Yunhua Xu*[a]

Organic batteries hold significant promise for large-scale applications due to their environmental friendliness and cost-effectiveness, but they face challenges such as active material dissolution and sluggish reaction kinetics, particularly at low temperatures. Here, we employ gel polymer electrolytes (GPEs) with an ultra-low concentration of 0.1 M to tackle these issues. The diluted GPEs effectively suppress the dissolution and migration of organic species, reduce electrolyte decomposition by forming a polymer-dominated solid-electrolyte interphase, lower the Li^+ de-solvation barrier, and enhance Li-ion diffusion under low-temperature conditions. The diluted GPEs demonstrate exceptional cycling stability and rate capability of organic batteries, achieving a cycle life of 1200 cycles at 2C and a high specific capacity of 101 mAh g^{-1} at an ultra-high 10C rate at −50 °C. Moreover, even at a high mass loading of 8 mg cm^{-2}, the battery exhibits excellent cycling performance, retaining 90.0% of its capacity after 500 cycles. Our findings significantly expand the applicability of organic batteries to extremely cryogenic environments while also reducing costs.

Received 21st November 2025
Accepted 12th January 2026

DOI: 10.1039/d5sc09108j

rsc.li/chemical-science

1 Introduction

Since the commercialization of lithium-ion batteries (LIBs) in 1991, they have become the dominant energy storage solution for portable electronic devices, electric vehicles and grid storage systems. With the continuous increase in demand for energy storage, there is a pressing need to develop high-performance LIBs with robust security features that can operate in harsh environments such as space exploration, polar expeditions, and underwater operations. However, conventional inorganic electrode materials employed in commercial LIBs often experience significant performance degradation at low temperatures, primarily attributed to sluggish intercalation/deintercalation kinetics and inadequate Li^+ diffusivity at electrode/electrolyte interfaces.[1–6] In contrast, organic electrode materials, which rely on conversion reactions of electrochemically active groups, offer a promising solution for creating low-temperature batteries with rapid reaction kinetics.[7–9] Nevertheless, major challenges remain due to the pronounced dissolution of organic redox species in organic liquid electrolytes and the inherently insulating nature of organic electrode materials, leading to notable capacity degradation and sluggish kinetics.[10,11] In addition, commercial organic liquid electrolytes are flammable and volatile, posing significant safety risks.[12,13]

In the pursuit of improved cycling performance and safety of organic batteries, the use of solid-state electrolytes (such as sulfide and polymer-based electrolytes) has been considered as a direct strategy to mitigate the dissolution of organic electrode materials.[14–17] However, organic batteries utilizing solid-state electrolytes often suffer significant capacity and power degradation at temperatures below 0 °C due to insufficient ion transport dynamics. This limitation represents a major obstacle for the practical deployment of organic batteries in cold climates. In addition, the strategy of employing high-concentration electrolytes has been recognized as effective in mitigating the dissolution of organic electrode materials.[18,19] Nonetheless, elevated salt concentrations lead to increased viscosity and decreased ionic conductivity of the electrolyte, resulting in sluggish reaction kinetics and inadequate electrochemical performance, particularly under cryogenic conditions. Moreover, the high cost and reduced wettability associated with high-concentration electrolytes make them impractical for widespread deployment (Fig. 1a).[20,21] Therefore, achieving a balance among high safety, long cycling lifespan, low cost, and stable operation at low temperatures through electrolyte engineering remains a significant challenge.

In recent years, there has been a surge in the development of low-concentration liquid electrolytes (LCEs) due to their notable advantages in cost reduction, expanded operational temperature ranges, and enhanced electrochemical performance.[22–27]

[a]School of Materials Science and Engineering, Key Laboratory of Advanced Ceramics and Machining Technology (Ministry of Education), Tianjin University, Tianjin 300072, China. E-mail: yunhua.xu@tju.edu.cn

[b]Institute of Technology for Carbon Neutrality, Shenzhen Institutes of Advanced Technology, Chinese Academy of Sciences, Shenzhen 518055, China

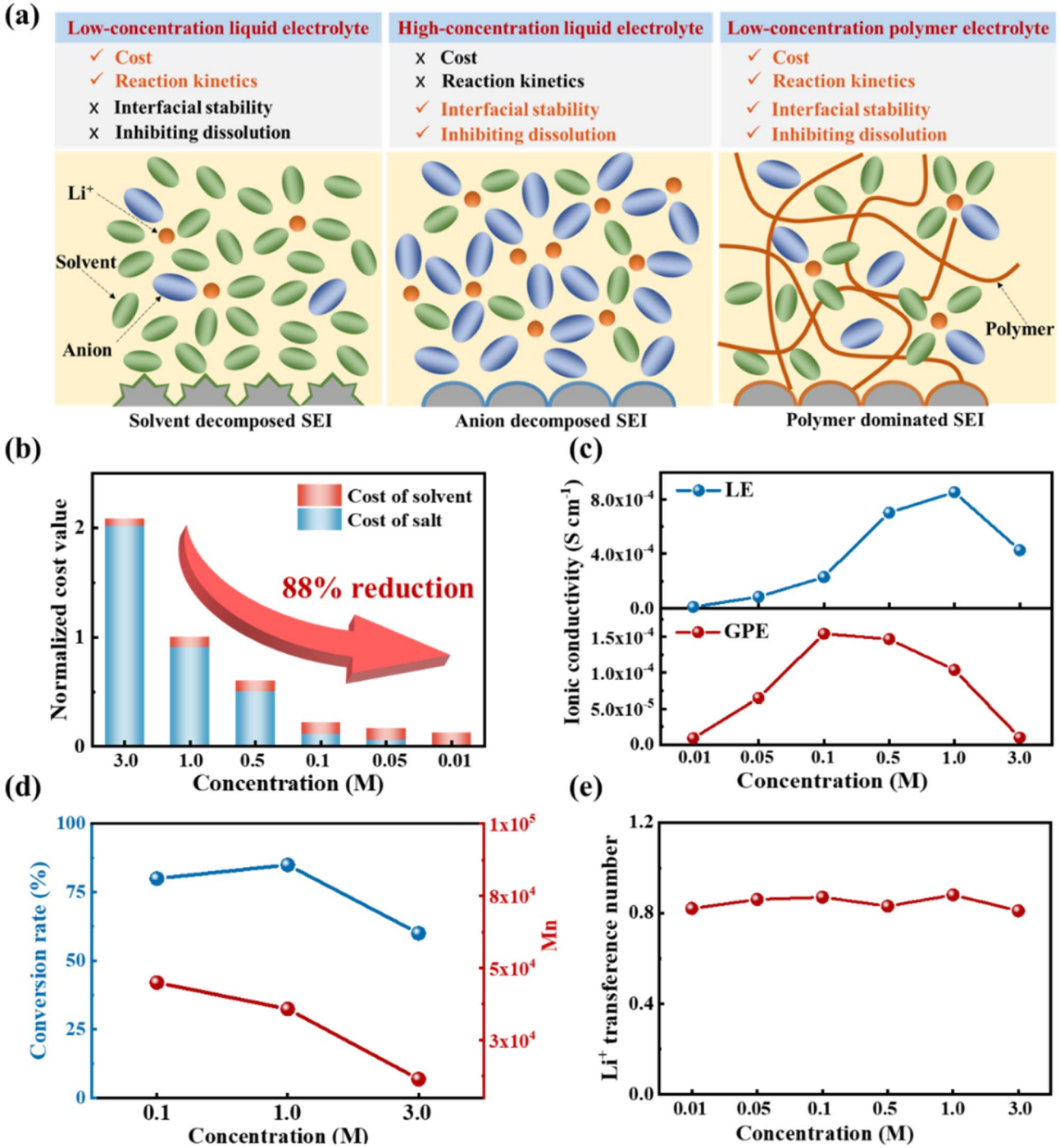

Fig. 1 (a) Schematic representations of various electrolyte systems. (b) Estimated electrolyte cost comparison for LEs with different salt concentrations. (c) Ionic conductivities comparison between LEs and GPEs. (d) Conversion rate of DOL to poly-DOL (PDOL) and the number-average molecular weight (M_n) of PDOL in GPEs. (e) Li-ion transference numbers of GPEs with different LiTFSI concentrations ranging from 0.01 M to 3.0 M.

Hu *et al.*[28] demonstrated that a LCE with a concentration of 0.3 mol L^{-1} (M) significantly extends the operating temperature range of Na-ion batteries (−30 to 55 °C). This is attributed to its low viscosity at reduced temperatures and a diminished risk of corrosion at elevated temperatures. Additionally, LCEs have been demonstrated to mitigate the dissolution and shuttle effect of polysulfides, leading to substantial improvements in the cycling stability and rate performance of Li–S batteries at room temperature.[29] Notably, compared to the conventional concentration of 1.0 M used in commercial electrolytes, Li–S batteries employing 0.1 M LCE exhibited improved capacity utilization and accelerated reaction kinetics under low-

temperature conditions.[30] More recently, Yan *et al.*[31] uncovered that LCEs can enhance Li^+ de-solvation kinetics, thereby improving the performance of Li–S batteries at cryogenic conditions. Although the strategic design of LCEs holds significant promise for addressing the challenges and achieving high-performance outcomes of organic batteries at low temperatures, using LCEs in organic batteries is challenging due to the concerns that they may compromise cycling stability by exacerbating dissolution and shuttling effects (Fig. 1a).[32]

Here, we introduce ultra-low concentration gel polymer electrolytes (GPEs) for low-temperature lithium–organic batteries. These GPEs, characterized by their ultra-low concentration, significantly reduce the Li^+ de-solvation barrier and enhance Li-ion diffusion at low temperatures. Concurrently, the formation of thin and stable solid-electrolyte interphase (SEI) layers greatly improves reaction kinetics. Moreover, the dilute GPEs effectively mitigate the dissolution and shuttling of active organic species through a synergetic effect of charge repulsion and physical confinement. These advancements promote stable cycling and high-rate performance at low temperatures, resulting in an impressive cycle life of 1200 cycles at 2C, along with a specific capacity of 101 mAh g^{-1} at an ultra-high 10C rate at −50 °C. Even under challenging conditions with a high cathode mass loading of 8 mg cm^{-2}, a stable reversible capacity of 190 mAh g^{-1} is maintained after 500 cycles. The implementation of ultra-low concentration electrolytes would extend the applicability of organic batteries to exceedingly cryogenic environments while substantially reducing costs.

2 Results and discussion

2.1 Characterization of the electrolytes with varing salt concentrations

A remarkable advantage of LCEs is the reduction in electrolyte material cost, primarily due to the lower consumption of expensive lithium salts. Compared to a conventional 1.0 M electrolyte, the estimated electrolyte-cost reduction is 40% for the concentration of 0.5 M, 78% for 0.1 M, 87% for 0.05 M, and 88% for 0.01 M (Fig. 1b and Table S1). Assuming the electrolyte contributes ∼10% of the total cell cost, the 0.1 M LE is estimated to yield an overall cell-cost reduction of ∼7.8%, provided that all other cost components remain constant.[33] The impact of varying concentrations on the electrochemical properties of both liquid electrolytes (LEs) and GPEs were investigated. GPEs were synthesized *via* the ring-opening reaction of DOL with an *in situ* polymerization method.[34] LEs consist of the lithium salt of LiTFSI and mixed solvents of DOL and DME (1 : 1, v/v). As the ionic conductivity is closely related to the concentration and mobility of charge carriers in LEs,[35] both the reduced number of ionic carriers in LCEs and the increased viscosity of high-concentration electrolytes can lower the ionic conductivity. The LE exhibits the highest ionic conductivity at 1.0 M (Fig. 1c and S1a), consistent with previous reports.[20,36,37] In contrast, in GPEs, the electrolyte at 0.1 M demonstrates a higher ionic conductivity of 1.6×10^{-4} S cm^{-1} comparable with the 1.0 M electrolyte (Fig. 1c and S1b). Even under low-temperature conditions, 0.1 M GPE still exhibits higher ionic conductivity and lower activation energy for ionic conduction (Fig. S2). The polymerization of DOL was investigated using ^1H nuclear magnetic resonance (NMR) and Raman spectroscopy (Fig. S3 and S4). Through NMR peak integration, the conversion rates of DOL to poly-DOL (PDOL) were measured at 80% for 0.1 M GPE and 85% for 1.0 M GPE. At a further elevated concentration of 3.0 M, however, the conversion rate decreased to 60% (Fig. 1d). This decrease is mainly attributed to the markedly higher viscosity of the 3.0 M precursor LE before gelation, which reduces the diffusion of DOL and oligomer species to the Nafion-coated separator and thus slows the ring-opening polymerization. As shown in Fig. S4b, the ring-stretching vibration of DOL disappears in the Raman spectrum for the 0.1 M GPE compared to those of PDOL and the 0.1 M LE system. At the same time, the C–O and CH_2 vibrations associated with the linear PDOL appear, indicating the ring-opening polymerization of DOL.[38] Furthermore, GPEs with varying salt concentrations exhibit notably high Li-ion transference numbers (>0.8), exceeding those reported for previously reported PDOL-based GPEs (Fig. 1e and S5).[39] This enhancement is mainly attributed to the ion-selective, anion-repelling Nafion layer coated on the separator, where fixed sulfonate groups ($-SO_3^-$) suppress anion transport and preferentially facilitate Li^+ migration.

2.2 Electrochemical performance comparison of organic and inorganic cathodes in GPEs

The advantages of low-concentration GPEs are further highlighted through comparing the electrochemical performance of organic and inorganic cathodes. As representatives, 1,3,5-tri(9,10-anthraquinonyl)benzene (TAQB) and lithium iron phosphate ($LiFePO_4$, LFP) were utilized as the cathode materials. To elucidate the specific benefits imparted by the GPEs, we performed a direct comparison between the 0.1 M GPE and 0.1 M LE with an identical salt/solvent composition. As shown in Fig. S6, the TAQB-Li cell with 0.1 M LE delives an initial discharge capacity comparable to that of the 0.1 M GPE at room temperature. However, it suffers from rapid capacity fading, retaining only 26.4% of its capacity after 200 cycles. This accelerated fading is consistent with enhanced dissolution and shuttling effect of organic molecules and redox intermediates in the liquid phase, which aggravates parasitic reactions and leads to progressive interfacial deterioration.[34] In contrast, the cell using 0.1 M GPE demonstrates markedly enhanced cycling stability, retaining 97% of its capacity after 200 cycles (Fig. 2a). Notably, compared with the 1.0 M LE, the 1.0 M GPE also delivers substantially enhanced cycling stability. This improvement is attributed to the polymer network, which provides physical confinement to soluble molecules, thereby suppressing their dissolution and migration. Additionally, the Nafion-coated separator further impedes the migration of charged intermediates *via* charge repulsion, synergistically mitigating the shuttle effect.[34] These results collectively demonstrate that replacing the LE with GPE can effectively suppress shuttle reactions associated with organic electrodes while maintaining the electrochemical performance, thereby enabling durable and stable cycling. We further evaluated TAQB

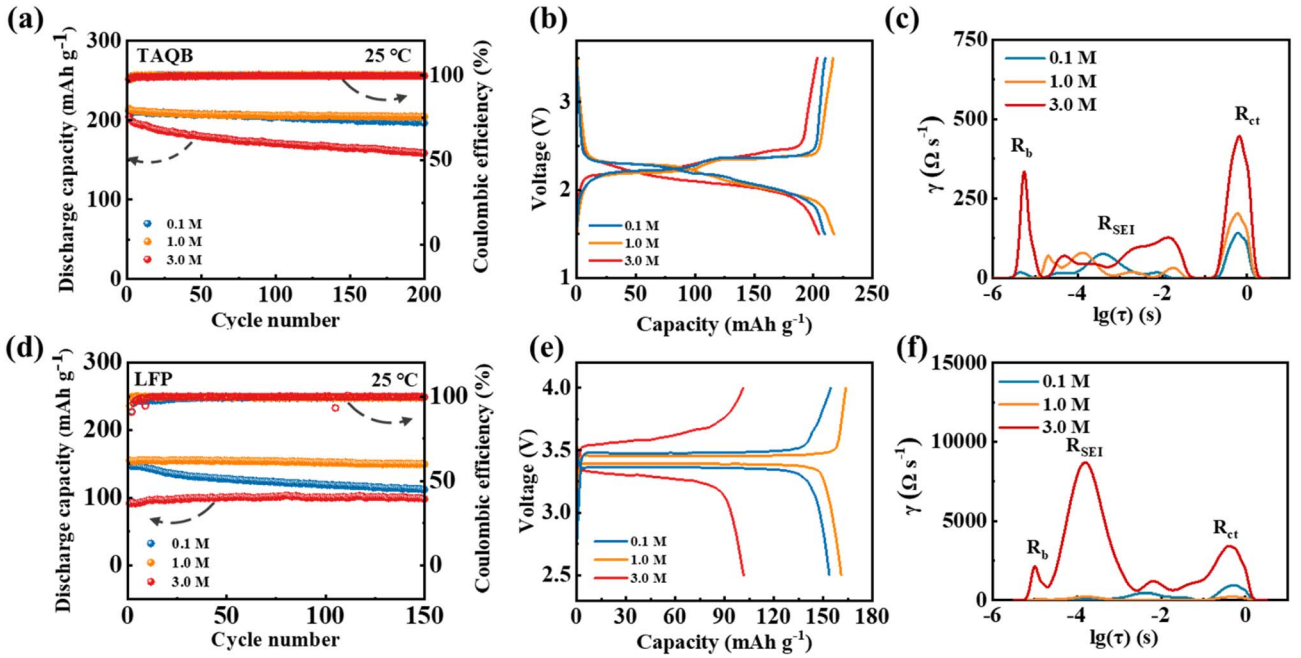

Fig. 2 Electrochemical performance comparison of TAQB-Li and LFP-Li batteries utilizing GPEs with varying LiTFSI concentrations of 0.1, 1.0, and 3.0 M at 0.5C and 25 °C. (a and d) Cycling performance, (b and e) charge–discharge profiles, (c and f) corresponding DRT plots derived from EIS data collected over the frequency range of 10^6 to 1 Hz for (a–c) TAQB-Li and (d–f) LFP-Li batteries.

cycling across a wide GPE concentration range to assess the generality of the GPE-enabled stabilization. Across the GPE concentrations ranging from 0.01 to 1.0 M, TAQB exhibited consistent cycling stability with near-100% coulombic efficiency, as depicted in Fig. 2a and S7, and detailed in Table S2. Particularly noteworthy is the exceptional performance observed at an extremely low concentration of 0.01 M, where a high initial specific capacity of 190 mAh g^{-1} was achieved, with 87.3% retention after 200 cycles. Notably, such performance at such a low concentration has not been previously reported. The slightly lower initial specific capacity in the 0.01 M GPE can be reasonably ascribed to the combined effects of increased polarization due to low ionic conductivity and partial dissolution of lithiated TAQB into the residual liquid-like phase (Fig. S7). Conversely, at an elevated concentration of 3.0 M, TAQB shows inferior performance, with a lower initial specific capacity and reduced capacity retention of 80% after 200 cycles. The performance degradation is attributed to two synergistic effects: the high-concentration GPE not only induces sluggish Li^+ transport, but also exacerbates interfacial side reactions, while the reduced polymerization conversion of DOL and lower molecular weight of PDOL compromise its ability to suppress soluble organic molecules (Fig. 1d), thereby accelerating active material loss and capacity decay. Furthermore, GPEs with concentrations ranging from 0.01 to 1.0 M exhibited low voltage polarizations, whereas those at 3.0 M displayed significantly larger polarizations (Fig. 2b), indicating improved kinetics at lower concentrations.

The Nyquist plots of TAQB-Li batteries employing GPEs with varying salt concentrations were further transformed into distribution of relaxation time (DRT) curves to assess the impedance contributions of individual components intuitively (Fig. 2c and S8a). The peaks appearing in the relaxation time range of 10^{-6} to 10^{-4} s correspond to Li^+ transport within the electrolyte, those between 10^{-4} and 10^{-2} s are associated with the charge transfer of Li^+ across the SEI, and peaks within the range of 10^{-2} to 10 s represent the charge transfer process at the electrode interface.[40,41] The results reveal that, compared to the 0.1 M and 1.0 M GPEs, the high-concentration salt GPE exhibits significantly increased bulk impedance, solid electrolyte interphase resistance (R_{SEI}), and charge transfer resistance (R_{ct}). These increases are likely attributed to the combined effects of inhibited ion migration at high salt concentration, excessive accumulation of salt decomposition by-products, and a denser solvation structure that raises the desolvation energy barrier.

LFP exhibits markedly distinct electrochemical performance. With the 1.0 M GPE, stable cycling is achieved, along with typical charge/discharge voltage profiles, which can be attributed to its moderate ionic conductivity and a stable electrode/electrolyte interface (Fig. 2d). However, at a low concentration of 0.1 M, LFP shows rapid capacity decay owing to the limited high-voltage stability of the dilute electrolyte (Fig. S9). The applied cutoff voltage of 4.0 V induces irreversible electrolyte decomposition, which contributes to a significant increase in interfacial impedance (Fig. 2f). It is worth noting that at 3.0 M, the capacity drops substantially to 91.8 mAh g^{-1} (Fig. 2d and Table S3), accompanied by a markedly pronounced polarization and increased resistance, indicative of hindered interfacial kinetics and elevated barriers for Li^+ transport across the electrode/electrolyte interface (Fig. 2e and f). Meanwhile, the mass transport resistance arising from the high-viscosity environment hindered the one-dimensional diffusion of Li^+ in

the olivine structure. Consistent with the voltage-window limitation proposed above, a low-voltage inorganic cathode ($Li_4Ti_5O_{12}$) exhibits stable cycling in both 0.1 M and 1.0 M GPEs, whereas the 3.0 M GPE suffers from excessive polarization (Fig. S10). Therefore, low-concentration GPEs offer clear advantages for organic cathodes by suppressing dissolution and shuttle reactions. For inorganic cathodes, their compatibility is largely governed by the operating voltage window. Stable performance can be achieved in low-voltage systems, whereas application to high-voltage cathodes may require further improvement in oxidative stability.

2.3 Li deposition morphology and interfacial chemistry in GPEs

To gain insight into the cycling stability of TAQB in low-concentration GPEs, the morphology of the electrodes and separators after 200 cycles was examined using scanning electron microscopy (SEM). As illustrated in Fig. S11, the surfaces of the TAQB cathodes employing the dilute (0.1 M) and regular (1.0 M) electrolytes were completely coated with the *in situ* formed PDOL. Correspondingly, the respective separators retained their original white color, indicating effective prevention of TAQB shuttling. This observation aligns with the battery's exceptional cycling stability using these electrolytes. In contrast, the TAQB cathode using the 3.0 M GPE exhibited partial polymer coverage due to the low conversion rate of DOL to PDOL. This results in an insufficient blocking effect, leading to noticeable capacity degradation after 200 cycles.

Furthermore, the cycled Li metal anode with the 0.1 M GPE demonstrates a uniform, smooth surface and a dense, thin passivation layer of 20 μm, indicating a homogeneous and dense Li deposition during cycling (Fig. 3a and b). However, with increasing salt concentration, the cycled Li anode surfaces exhibit pronounced cracking and randomly accumulated Li metallic grains, accompanied by a loose and thickened interfacial layer (Fig. 3c–f). Furthermore, as the cycling advances, the interfacial layer on the cross-section of the Li anode in the 3.0 M GPE progressively thickens, reaching approximately 250 μm after 500 cycles, accompanied by evident cracks (Fig. S12). This phenomenon is mainly attributed to severe dendrite growth, which induces extensive dead Li formation and continuous electrolyte consumption.[42] These results suggest an inadequate barrier against the TAQB shuttling and an unstable interface with the Li anode in the 3.0 M GPE. In contrast, the 0.1 M GPE successfully suppresses the soluble TAQB shuttling and facilitates the formation of a stable interfacial layer between the electrolyte and Li anode.

The stability of the TAQB cathodes in GPEs with different concentrations was investigated using EIS measurements after various cycles. Nyquist plots with fitted curves and equivalent electrical circuits are shown in Fig. S13. In the 0.1 M GPE, the R_{SEI} and R_{ct} remain stable at low values during cycling, indicating the formation of a stable SEI layer and a low-resistance charge-transfer process. Conversely, the resistances in the 1.0 M and 3.0 M GPEs undergoes a noticeable increase over cycling due to the continuous SEI growth. For the 3.0 M GPE, R_{SEI} increases from the initial 208 Ω to 742 Ω, while R_{ct} increases from 590 Ω to 1403 Ω after 200 cycles, revealing unstable interfacial contact and sluggish reaction kinetics. The EIS results suggest that low-concentration GPEs facilitate optimized SEI formation and improved kinetics.

The effects of concentration on the Li metal anodes were investigated by examining the compositions of the SEI formed in the GPEs with different concentrations using X-ray photoelectron spectroscopy (XPS). The Li metal anodes were retrieved from cycled cells. As illustrated in Fig. S14, the F contents of the SEI layers corresponding to the 0.1, 1.0, and 3.0 M GPEs are 6.5 at%, 10.4 at%, and 13.7 at%, respectively. The F 1s spectra display two peaks at 688.4 and 684.8 eV, corresponding to the C–F species and LiF, respectively (Fig. 3g). To quantify the LiF contribution more rigorously, we normalized the peak areas within the F 1s envelope. With decreasing concentration from 3.0 to 0.1 M, the LiF fraction dropped from 20.22% to 7.65%. This trend demonstrates that the contribution of LiF-type inorganic fluorinated species becomes progressively more pronounced with increasing salt concentration, whereas the dilute 0.1 M GPE yields a much lower LiF contribution among F-containing species, suggesting a reduced formation of LiF-rich inorganic products at lower concentrations. Although the LiF has a high binding energy with Li and may promote uniform Li^+ deposition, it has a low ionic conductivity of 10^{-31} S cm^{-1}, leading to high resistance and increased polarization.[43–46] The C 1s spectra show that a large amount of organic species is formed in the SEI (Fig. 3h). The peaks at 284.8, 286.3, 288.6, 289.8, and 292.4 eV are assigned to C–C/C–H, C–C–O, O–C–O, COOR, and C–F groups, respectively.[38] The stronger C–C–O and O–C–O peaks for the 0.1 M GPE indicate more PDOL is produced, forming an elastic polymer-dominated SEI layer and thereby a stable interface layer. With increasing concentration, the SEI layer gradually transitions into a mixture of organic and inorganic species, rendering an unstable SEI layer during cycling. Thus, the low-concentration GPEs produce a flexible, and structurally uniform SEI film, protecting the Li anode from dendrite growth (Fig. 3i).

2.4 Lithium-ion diffusion of organic and inorganic cathodes in GPEs

The impacts of electrolyte concentration on the reaction kinetics and ionic transport behavior of the TAQB and LFP cathodes were investigated through cyclic voltammetry (CV) and galvanostatic intermittent titration technique (GITT) measurements. CV results show that the kinetics of the TAQB cathode in the 1.0 M GPE are predominantly governed by a surface-controlled capacitive process (Fig. S15). As a reduced electrolyte concentration of 0.1 M, the capacitive process still maintained a high contribution, demonstrating favorable oxidation–reduction reaction kinetics (Fig. 4a and b). The apparent diffusion coefficient of Li ions (D_{Li^+}) for TAQB cathodes was calculated using the Randles–Sevcik equation (Fig. S16), with values summarized in Table S4. For the 0.1 and 1.0 M GPEs, TAQB exhibited similar D_{Li^+} values ranging from 10^{-9} to 10^{-11} cm^2 s^{-1}, suggesting that the overall kinetics associated with its

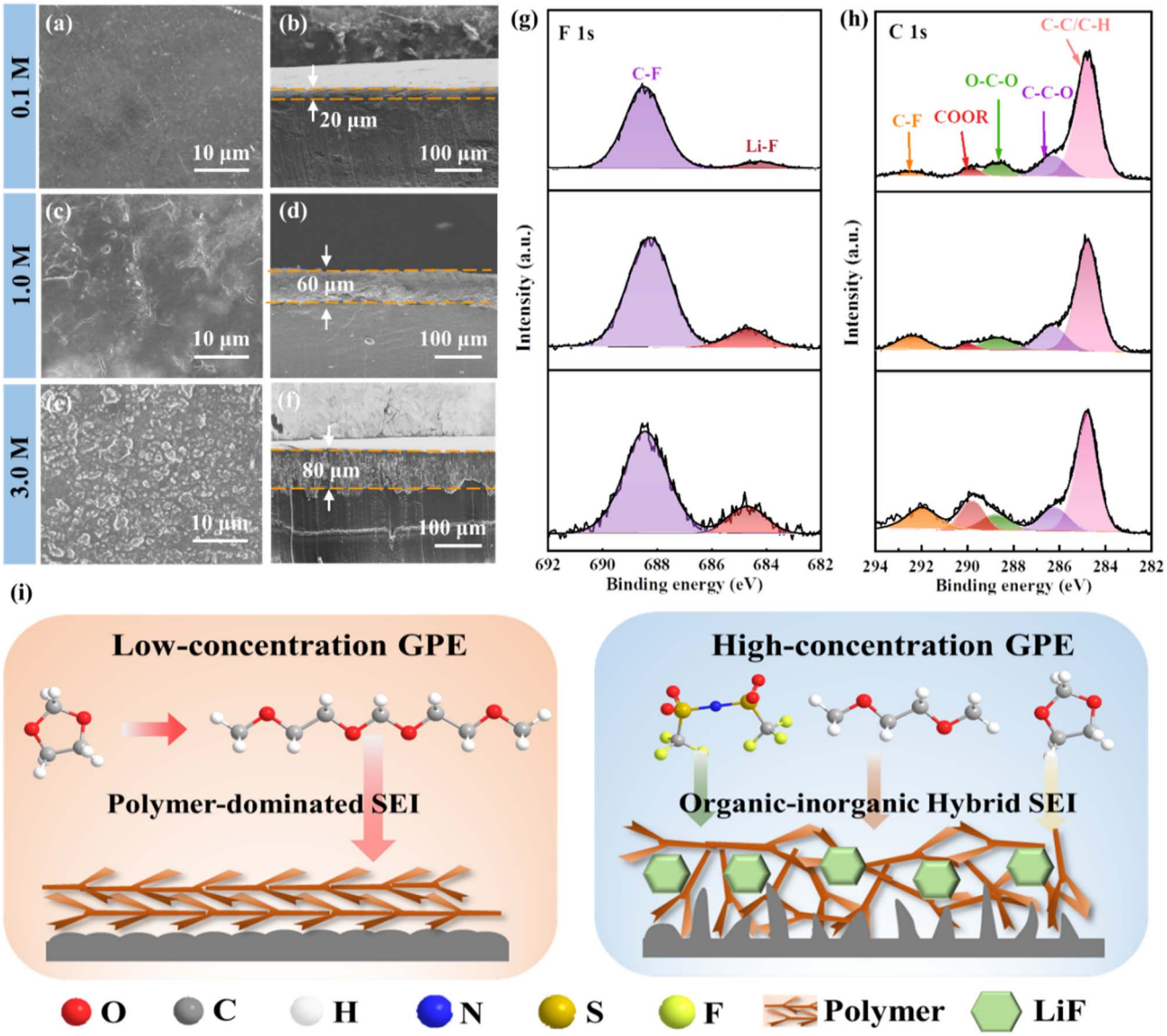

Fig. 3 Impacts of electrolyte concentrations on Li anodes in TAQB-Li batteries after 200 cycles. SEM images of the (a, c and e) surface and (b, d and f) cross-section and XPS spectra of (g) F 1s and (h) C 1s of the cycled Li anodes using different concentration GPEs. (i) Schematic diagrams of the SEI formation and decomposition of low- and high-concentration GPEs.

charge storage are not significantly compromised in low-concentration electrolytes (Fig. 4c). In contrast to the fast capacitive-dominated Li-storage process observed in TAQB electrodes, Li^+ storage in LFP is predominantly diffusion-controlled (Fig. S17). Accordingly, the CV-derived D_{Li^+} for the LFP electrode is markedly higher in the 1.0 M GPE than in the 0.1 M GPE (Fig. S18 and Table S5), indicating a stronger concentration dependence of its apparent diffusion kinetics. The difference in reaction kinetics between the organic and inorganic cathodes in different concentration GPEs is also highlighted by GITT measurements. It should be noted that, for pseudocapacitive electrodes, the D_{Li^+} values obtained from GITT may not fully represent the intrinsic bulk diffusion coefficient of the active material, because the voltage relaxation is often coupled with surface redox equilibration and double-layer charging in addition to ion transport. Nevertheless, when the same electrode material is prepared under identical conditions, the GITT-derived D_{Li^+} can still serve as an effective descriptor to compare the apparent Li^+ transport kinetics within the composite electrode across different electrolytes. As illustrated in Fig. 4d and S19, comparable D_{Li^+} values are calculated from GITT for the TAQB electrode in the 0.1 and 1.0 M GPEs. However, LFP displayed a significantly higher D_{Li^+} in the 1.0 M GPE than in the 0.1 M GPE (Fig. 4e and S20), consistent with the CV measurement results. Notably, a relatively high D_{Li^+} was obtained at low temperatures of −20 and −50 °C with the 0.1 M GPE for the TAQB electrode, promising retained kinetic performance under cold conditions (Fig. 4f and S21).

The discrepancy in reaction kinetics at low concentrations between organic and inorganic cathodes can be attributed to

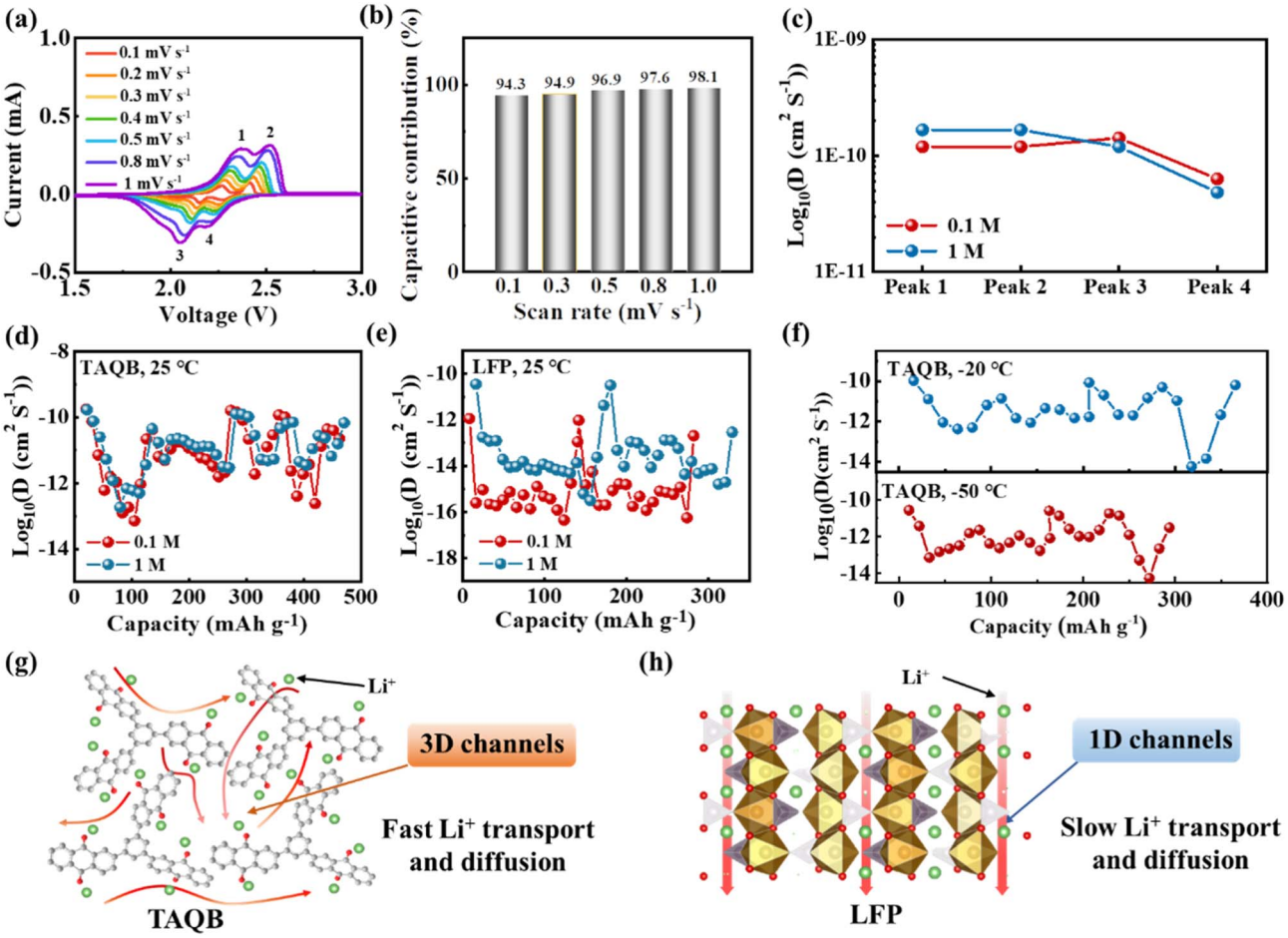

Fig. 4 Analysis of the electrochemical behavior of the TAQB and LFP cathodes using GPEs with LiTFSI concentrations of 0.1 and 1 M. (a) CV curves and (b) capacitive contributions of the TAQB electrode at different scan rates with the 0.1 M GPE. (c) The Li-ion diffusion coefficients of the TAQB electrode with 0.1 and 1 M GPEs based on Randles–Sevick equation. Li-ion diffusion coefficients calculated from GITT measurements in (d) TAQB and (e) LFP electrodes at 25 °C using the 0.1 and 1 M GPEs. (f) Li-ion diffusion coefficients calculated from GITT measurements in TAQB electrode at −20 and −50 °C using the 0.1 M GPE. Schematic diagram illustrating the difference in Li^+ diffusion pathways between (g) TAQB and (h) LFP electrodes.

their distinct charge storage mechanisms. The capacity of TAQB is primarily contributed by the surface-controlled pseudocapacitive process with rapid reaction kinetics. Density functional theory (DFT)-based structural optimization reveals that the TAQB molecule adopts a stable propeller-like three-dimensional conformation in its lowest energy state, where the three anthraquinone units exhibit a distinctly non-planar arrangement (Fig. S22a). This spatial steric hindrance generates abundant intermolecular voids, which can facilitate the rapid transport of Li^+. Furthermore, molecular dynamics (MD) simulations on multiple organic molecules in their lithiated states demonstrated that the propeller-like structure remains stable upon lithiation (2Li-TAQB). As shown in Fig. S22b, the simulation snapshots revealed that the active sites of the coordinated Li^+ are distributed in a three-dimensional, anisotropic manner, providing an optimized diffusion pathway for electrolyte penetration and Li^+ migration. Even at low concentrations, there are still sufficient Li^+ involved in the reaction due to the abundant active sites on the organic electrode materials and the three-dimensional diffusion pathway of Li^+ (Fig. 4g). In contrast, the olivine-structured $LiFePO_4$ exhibits intrinsically limited Li^+ diffusion kinetics due to its one-dimensional transport channels oriented along the [010] crystallographic direction (Fig. 4h).[47] The combined effect of the reduced Li^+ concentration in the 0.1 M GPE and the inherent long-range transport bottlenecks of the one-dimensional channels leads to a decrease of D_{Li^+} within the electrode and pronounced electrode polarization (Fig. 2e). This process further lowers the utilization of active materials and accelerates capacity fading during cycling (Fig. 2d). These findings indicate that the low-concentration GPEs hold promise for use in organic batteries without adversely affecting reaction kinetics.

2.5 Effects of salt concentration and temperature on lithium-ion desolvation in GPEs

Considering that the Li^+ solvation structure significantly influences reaction kinetics, the impact of salt concentration on the Li^+ solvation structure in GPEs was investigated using MD

simulations and DFT analysis at varying temperatures. To mimic the polymer matrix, chains comprising 10 repeating units of –C–C–O–C–O– were utilized instead of PDOL. The MD simulation snapshots of these systems at 25 and −50 °C are depicted in Fig. 5a–d.

To elucidate the temperature- and concentration-dependent Li^+ transport mechanisms, the radial distribution function ($g(r)$) and coordination number (CN) of Li^+ in the two electrolytes at 25 and −50 °C were quantitatively evaluated *via* MD simulations. As shown in Fig. 5e and f, and S23, within the first solvation shell of Li^+ (≤3 Å), DOL molecules contribute minimally to Li^+ coordination, and the Li^+ solvation environment is primarily composed of PDOL, $TFSI^-$, and DME, which is consistent with the Raman results. Quantitative coordination analysis at −50 °C revealed that in the 0.1 M GPE, each Li^+ is coordinated by an average of 3.4 PDOL oxygens, 0.6 $TFSI^-$ oxygens, and 1.9 DME oxygens (Fig. 5e). Notably, increasing the electrolyte concentration to 1.0 M significantly decreased the coordination number of PDOL oxygens to 2.1, while that of $TFSI^-$ increased to 1.9 (Fig. 5f). Therefore, as the salt concentration in the GPEs decreases, the total coordination number of Li^+ with solvent molecules in the first solvation sheath gradually increases, while the coordination number of Li^+ with $TFSI^-$ correspondingly decreases. This concentration-dependent transformation in the solvation structure reduces the fraction of Li^+–$TFSI^-$ contact ion pairs (CIPs) and promotes salt dissociation, leading to a higher proportion of mobile Li^+. At the same time, Li^+ can migrate *via* coordination with ether-oxygen groups along the continuous network formed by the polymer matrix, potentially offering additional diffusion pathways for Li^+.[48,49] As a result, compared to the 1.0 M GPE, the 0.1 M GPE exhibits a higher ionic conductivity (Fig. 1c). Moreover, PDOL tends to aggregate at the interface, forming highly flexible polymeric components, which enhances the elasticity and mechanical durability of the SEI film, as evidenced by the XPS analysis of the polymer-dominated SEI in the 0.1 M GPE (Fig. 3i).

To further elucidate the intrinsic correlation between solvation structure and de-solvation kinetics, the de-solvation free energy of representative Li^+ solvation configurations was

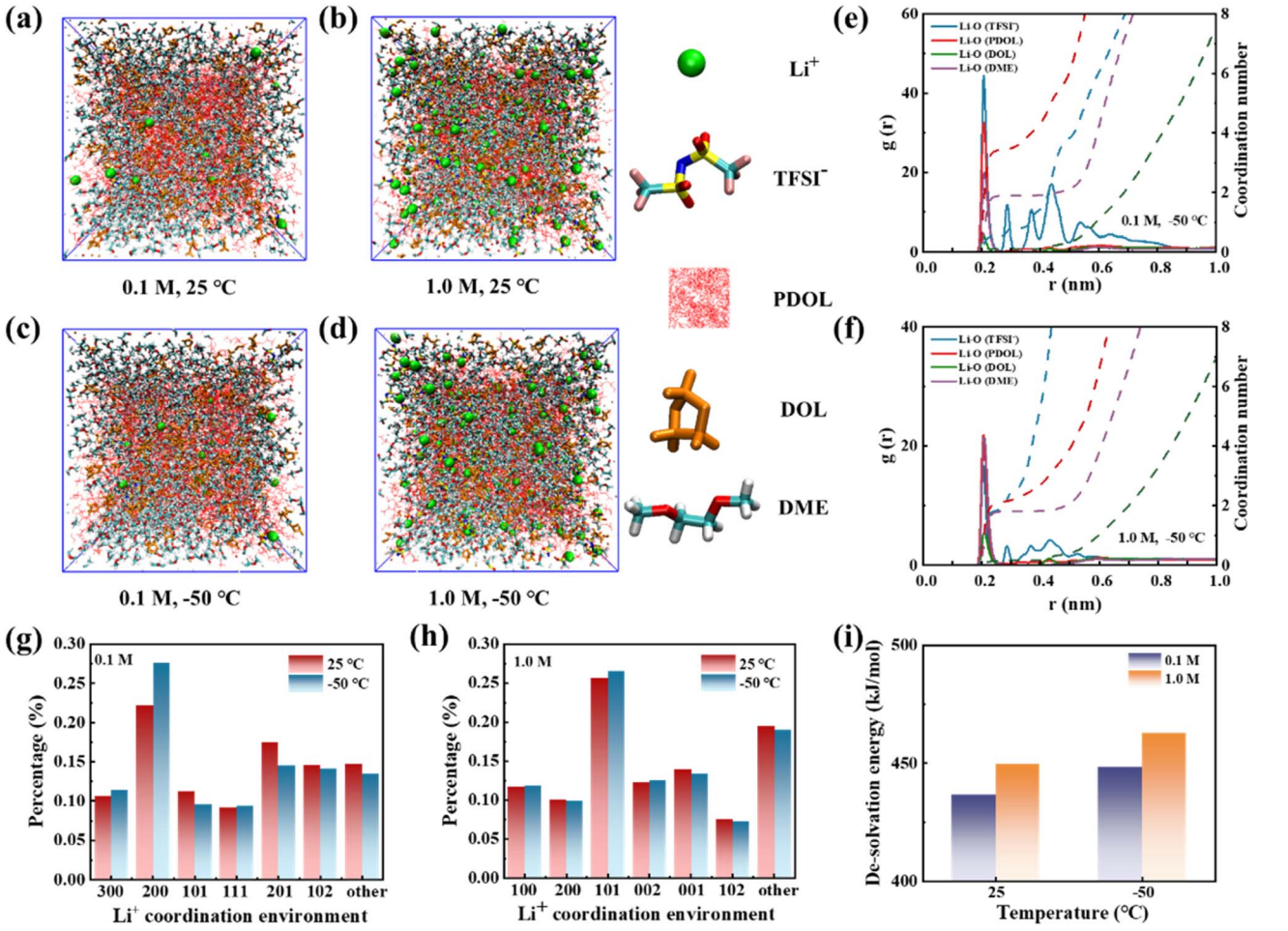

Fig. 5 Comparison of solvation structures in the 0.1 and 1.0 M GPEs at different temperatures. Snapshots obtained from MD simulations of the (a and c) 0.1 and (b and d) 1.0 M GPEs at (a and b) 25 °C and (c and d) −50 °C. Radial distribution functions (RDF) and corresponding coordination numbers of the (e) 0.1 and (f) 1.0 M GPEs at −50 °C. The distribution of various Li^+ coordination environment in the (g) 0.1 and (h) 1.0 M GPEs at 25 °C and −50 °C (here *xyz* represents one Li^+ with *x* PDOL, *y* DOL, and *z* DME around 0.3 nm). (i) Average Li^+ de-solvation energies in different GPEs at 25 °C and −50 °C.

quantified *via* DFT calculations (Tables S6 and S7). Partial solvation configurations of Li^+ in GPE are illustrated in Fig. S24. Based on the relative abundances of various Li^+ solvation structures in GPE at both room and subzero temperatures (Fig. 5g and h), the average de-solvation free energies were calculated for different salt concentrations. The outcomes depicted in Fig. 5i reveal that, at both 25 and −50 °C, the average de-solvation free energy in the 0.1 M GPE is markedly lower than that in the 1.0 M GPE. This result suggests that, under both ambient and cryogenic conditions, reducing the salt concentration effectively lowers the energy barrier for Li^+ desolvation and promotes reaction kinetics across a wide temperature range.

The EIS of symmetric lithium batteries at various temperatures were analyzed *via* the DRT technique to quantify the impedance contributions of each component in electrolytes of varying salt concentrations (Fig. S25).[50,51] The R_{SEI} of the Li metal anode using the 0.1 M GPE was 6622 Ω at −10 °C, which was much lower than that of the Li metal anode using the 1.0 M GPE (9835 Ω). This could be attributed to the formation of the polymer-dominated SEI by the low-concentration GPE, which facilitates the transport of Li^+ along the polymer molecular chain segments within the SEI.[41] Additionally, based on the Arrhenius equation and EIS fitting results, the activation energy barrier for Li^+ diffusion through the SEI of the anode using the 0.1 M GPE was significantly lower than that of the anode using the 1.0 M GPE, indicating that the polymer-dominated SEI enables enhanced ionic transport kinetics (Fig. S25e). Furthermore, at −10 °C, the R_{ct} of the Li anode using the 0.1 M GPE was only one-third that of the 1.0 M GPE, suggesting fast Li^+ desolvation at the interface of the Li metal anode with the polymer-dominated SEI. Moreover, the de-solvation energy barrier of Li^+ in the 0.1 M GPE was lower than that in the 1.0 M GPE, which aligns with the simulation results (Fig. S25f). These findings collectively indicate that the low-concentration GPEs could accelerate Li^+ transport within the SEI, facilitate desolvation process, and significantly reduce the interfacial kinetic barrier, thereby promising superiorly improved battery performances at low temperatures.

Furthermore, the Li deposition morphology in GPEs with different salt concentrations at −50 °C was characterized to gain deeper insights into low-temperature interfacial stability. At a current density of 1 mA cm^{-2} and a plating/stripping capacity of 1 mAh cm^{-2}, the surface morphology of the Li metal after 50 cycles is presented in Fig. S26. In the 0.1 M GPE, the deposited Li layer exhibited a uniform and dense structure without obvious pore formation (Fig. S26a and b). In contrast, as the electrolyte concentration increased to 1.0 M, the deposited Li layer became significantly rougher, displaying a heterogeneous structure comprising blocky and dendritic features (Fig. S26c and d). When the concentration was further increased to 3.0 M, abundant dendritic structures were observed, with randomly stacked Li deposits forming a highly porous morphology, which increased the electrode–electrolyte interface and exacerbated interfacial side reactions (Fig. S26e and f).[52] These morphological changes are primarily attributed to the severely hindered Li^+ transport at the electrode interface under low-temperature conditions in high-concentration GPEs, promoting dendrite growth and dead Li formation. To further corroborate the above observations, atomic force microscopy (AFM) was performed on Li surfaces after 50 cycles at −50 °C (Fig. S27). The AFM results are consistent with the SEM analysis, showing a smooth and homogeneous Li surface in the 0.1 M GPE, whereas the 3.0 M system exhibits markedly increased roughness and pronounced surface undulations. Overall, these observations highlight that low-concentration GPEs can effectively facilitate uniform Li deposition and enhance interfacial stability under low-temperature conditions.

2.6 Superior environmental adaptability of organic batteries using low-concentration GPEs

To gain insight into the influence of the low-concentration GPEs on the electrochemical performance of organic batteries, the cycling and rate performance of TAQB were evaluated at room and low temperatures. As depicted in Fig. 6a, in the 0.1 M GPE, TAQB demonstrates an impressive capacity retention of 74.1% after 2000 cycles at 1C, mainly attributed to stable SEI formation and reduced dissolution and shuttling. Additionally, excellent rate performance is observed, with a remarkable specific capacity of 190 mAh g^{-1} achieved at an ultra-high current density of 50C (Fig. 6b). This corresponds to an elevated specific energy density of 380 Wh kg^{-1} and specific power density of 1900 W kg^{-1}. Notably, the voltage plateaus during charge/discharge remained consistent at varying current rates, attributed to the low charger transfer barrier, low de-solvation energy, and high D_{Li^+} within the organic batteries facilitated by the 0.1 M GPE (Fig. S28). To further evaluate the prospects of organic batteries in practical applications, the cycling performance of high-loading electrodes is also tested in the 0.1 M GPE. Even at a high TAQB loading of 8 mg cm^{-2}, a stable reversible capacity of 190 mAh g^{-1} with a high capacity retention of 90.0% can be obtained after 500 cycles (Fig. S29).

Remarkably, organic batteries employing the 0.1 M GPE exhibit superior low-temperature performance compared to those utilizing the 1.0 M GPE. Even at an extreme temperature of −70 °C, a high capacity of 133 mAh g^{-1} is retained in the 0.1 M GPE, equivalent to 63% of the capacity at 25 °C (Fig. 6c and d). Conversely, with the 1.0 M GPE, a rapid capacity decline occurs with decreasing temperature (Fig. S30a), dropping to 63.4 mAh g^{-1} at −70 °C, only 28% of the capacity at 25 °C. Actually, at temperatures below −30 °C, higher capacities are obtained in the 0.1 M GPE than in the 1.0 M GPE (Fig. 6c). Moreover, better voltage profiles are displayed with reduced polarization in the 0.1 M GPE compared to the 1.0 M GPE counterpart at low temperatures (Fig. 6d and S30b). Furthermore, the 0.1 M GPE demonstrates improved rate performance at low temperatures, with a high capacity retention of 101 mAh g^{-1} under a high rate of 10C at −50 °C (Fig. 6e and S31). In contrast, only 55 mAh g^{-1} is delivered for the 1.0 M GPE at 5C (Fig. S32). Impressively, at −50 °C, remarkably enhanced cycling stability is realized for the 0.1 M GPE with 84% capacity retention after 1200 cycles at 2C (Fig. 6f). Even at a high mass loading of 8 mg cm^{-2}, TAQB maintained stable cycling at −30 °C,

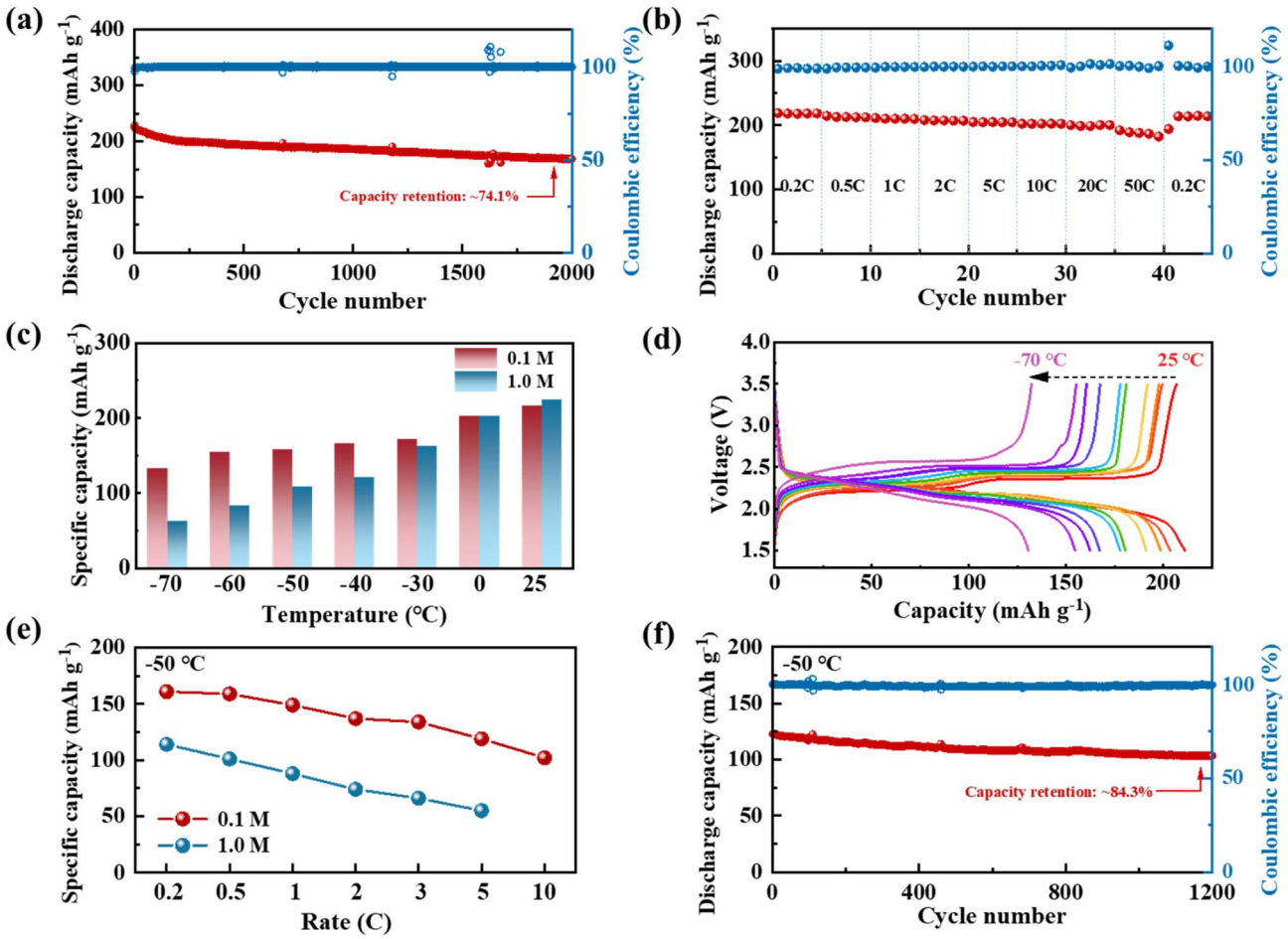

Fig. 6 Electrochemical performance of TAQB-Li batteries utilizing the 0.1 and 1.0 M GPEs. (a) Long-term cycling performance and (b) rate performance with the 0.1 M GPE at 25 °C. (c) Comparison of specific capacity in different GPEs. (d) Charge–discharge curves with the 0.1 M GPE at different temperatures ranging from 25 °C to −70 °C with a current density of 0.2C. (e) Comparison of the specific capacity between the 0.1 and 1.0 M GPEs at −50 °C with different current densities. (f) Long-term cycling performance with the 0.1 M GPE at −50 °C with a current density of 2C.

delivering a high capacity of 157.8 mAh g^{-1} after 50 cycles (Fig. S33). These results highlight that low-concentration GPEs can significantly enhance the cycling stability and rate capability of organic batteries under low temperatures.

To further investigate the kinetics disparity between 0.1 and 1.0 M GPEs, EIS measurements were conducted on the TAQB cathode at different temperatures (Fig. S34). Notably, with the 1.0 M GPE, R_{SEI} and R_{ct} increase substantially with declining temperature, attributed to ion/electron transport challenges at low temperatures. In contrast, the 0.1 M GPE exhibits consistently lower R_{SEI} and R_{ct} across a wide temperature range from 30 to −40 °C, aligning with its excellent rate and cycling performance at low temperatures. Specifically, at −40 °C, R_{ct} in the 1.0 M GPE is nearly five times higher than that in the 0.1 M GPE, indicating a lower de-solvation energy barrier of the low-concentration GPEs.[2,53] Consequently, reduced charge transfer barrier, improved Li^+ de-solvation kinetics and a high D_{Li^+} are key factors driving the enhanced electrochemical properties of the 0.1 M GPE at low temperatures.

3 Conclusions

In summary, low-concentration GPEs can realize exceptional cycling stability and rate capability in organic batteries operating at low temperatures. Low-concentration GPEs not only hold high Li^+ diffusion coefficient, fast charge-transfer kinetics, and low Li^+ de-solvation barrier at low temperatures, but also facilitate the formation of a polymer-dominated SEI layer to stabilize the Li anode and effectively suppress the dissolution of organic active materials. Consequently, Li-TAQB batteries with the 0.1 M GPE demonstrated a high specific capacity of 133 mAh g^{-1} at −70 °C, equivalent to 63% of its capacity at room temperature, and a notable rate performance with 101 mAh g^{-1} at an ultra-high rate of 10C and a long cycle life of 1200 cycles at 2C, even at a low temperature of −50 °C. Furthermore, at a high mass loading of 8 mg cm^{-2}, a stable reversible capacity of 190 mAh g^{-1} can be obtained after 500 cycles. Our findings present a promising solution for enabling rapid-charging organic batteries under extreme environments and could accelerate the

development of cost-effective and widely applicable energy storage systems.

4 Experimental section

Experimental details can be found in the SI.

Author contributions

Mengjie Li: writing-original draft, validation, methodology, investigation, formal analysis, data curation. Hang Liu: validation, software, investigation. Hai Su: methodology, investigation, data curation. Zehui Fan: software, investigation. Yuansheng Liu: data curation, conceptualization. Wei Zhu: software, investigation. Qinghao Chen: investigation. Jixing Yang: project administration, funding acquisition, conceptualization. Yunhua Xu: writing-review & editing, supervision, funding acquisition, conceptualization.

Conflicts of interest

There are no conflicts to declare.

Data availability

All the data supporting this article have been included in the main text and the supplementary information (SI). Additional data are available from the corresponding author upon reasonable request. Supplementary information: detailed materials and cell fabrication procedures, electrolyte preparation protocols, electrochemical measurement conditions and calculation methods (ionic conductivity, t_{Li^+}, D_{Li^+} from CV/GITT, and desolvation energy analysis), theoretical simulations (MD and DFT-based desolvation free-energy evaluation), additional tables, and extensive supplementary characterizations (SEM, XPS, ^{1}H NMR, GPC, Raman, EIS/DRT, CV, and GITT) that support the conclusions of this work. See DOI: https://doi.org/10.1039/d5sc09108j.

Acknowledgements

This work was supported by the National Natural Science Foundation of China (No.: 22579126, 52403283, 52273213, 22179092), National Postdoctoral Program for Innovative Talents (BX20240401), and China Postdoctoral Science Foundation (2023M743669).

References

1 B. Liao, H. Li, M. Xu, L. Xing, Y. Liao, X. Ren, W. Fan, L. Yu, K. Xu and W. Li, *Adv. Energy Mater.*, 2018, **8**, 1800802.
2 Y. Yang, Z. Li, M. Zhang, J. Wang, Y. Wang, J. Qiu and H. Zhao, *Adv. Mater.*, 2025, **37**, 2417981.
3 A. Gupta and A. Manthiram, *Adv. Energy Mater.*, 2020, **10**, 2001972.
4 X. Dong, Y. Wang and Y. Xia, *Acc. Chem. Res.*, 2021, **54**, 3883.
5 N. Zhang, T. Deng, S. Zhang, C. Wang, L. Chen, C. Wang and X. Fan, *Adv. Mater.*, 2022, **34**, 2107899.
6 A. Wang, Y. Song, Z. Zhao, X. Li, Z. Hu and J. Luo, *Adv. Funct. Mater.*, 2023, **33**, 2302503.
7 X. Dong, Z. Guo, Z. Guo, Y. Wang and Y. Xia, *Joule*, 2018, **2**, 902.
8 Z. Guo, J. Huang, X. Dong, Y. Xia, L. Yan, Z. Wang and Y. Wang, *Nat. Commun.*, 2020, **11**, 959.
9 J. Qin, Y. Liu, G. Li, Q. Lan, Z. Song, X. Ai and H. Zhan, *Adv. Energy Mater.*, 2024, **14**, 2400731.
10 M. Li, R. P. Hicks, Z. Chen, C. Luo, J. Guo, C. Wang and Y. Xu, *Chem. Rev.*, 2023, **123**, 1712.
11 Y. Shi, J. Yang, J. Yang, Z. Wang, Z. Chen and Y. Xu, *Adv. Funct. Mater.*, 2022, **32**, 2111307.
12 L. S. De Vasconcelos, R. Xu, Z. Xu, J. Zhang, N. Sharma, S. R. Shah, J. Han, X. He, X. Wu, H. Sun, S. Hu, M. Perrin, X. Wang, Y. Liu, F. Lin, Y. Cui and K. Zhao, *Chem. Rev.*, 2022, **122**, 13043.
13 L. Ma, J. Zhao, M. Li, H. Su, Y. Li, Y. Liu, H. Liu and Y. Xu, *ACS Appl. Mater. Interfaces*, 2025, **17**, 18206–18216.
14 X. Zhou, Y. Zhang, M. Shen, Z. Fang, T. Kong, W. Feng, Y. Xie, F. Wang, B. Hu and Y. Wang, *Adv. Energy Mater.*, 2022, **12**, 2103932.
15 Q. Ai, Z. Chen, B. Zhang, F. Wang, T. Zhai, Y. Liu, Y. Zhu, T. Terlier, Q. Fang, Y. Liang, L. Zhao, C. Wu, H. Guo, Z. Fan, M. Tang, Y. Yao and J. Lou, *ACS Energy Lett.*, 2023, **8**, 1107.
16 Z. Yang, F. Wang, Z. Hu, J. Chu, H. Zhan, X. Ai and Z. Song, *Adv. Energy Mater.*, 2021, **11**, 2102962.
17 X. Zhang, F. ying Shen, X. Long, S. Zheng, Z. Ruan, P. Cai, X. jia Hong and Q. Zheng, *Energy Storage Mater.*, 2022, **52**, 201.
18 K. Zhang, C. Guo, Q. Zhao, Z. Niu and J. Chen, *Adv. Sci.*, 2015, **2**, 1500018.
19 T. Cai, Y. Han, Q. Lan, F. Wang, J. Chu, H. Zhan and Z. Song, *Energy Storage Mater.*, 2020, **31**, 318.
20 Y. Yamada, J. Wang, S. Ko, E. Watanabe and A. Yamada, *Nat. Energy*, 2019, **4**, 269.
21 J. Holoubek, K. Kim, Y. Yin, Z. Wu, H. Liu, M. Li, A. Chen, H. Gao, G. Cai, T. A. Pascal, P. Liu and Z. Chen, *Energy Environ. Sci.*, 2022, **15**, 1647.
22 R. Glaser, F. Wu, E. Register, M. Tolksdorf, B. Johnson, J. Ready, M. Sanghadasa and G. Yushin, *J. Electrochem. Soc.*, 2020, **167**, 100512.
23 H. Zheng, H. Xiang, F. Jiang, Y. Liu, Y. Sun, X. Liang, Y. Feng and Y. Yu, *Adv. Energy Mater.*, 2020, **10**, 2001440.
24 G. Ma, L. Miao, W. Yuan, K. Qiu, M. Liu, X. Nie, Y. Dong, N. Zhang and F. Cheng, *Chem. Sci.*, 2022, **13**, 11320.
25 T. Liu, H. Li, J. Yue, J. Feng, M. Mao, X. Zhu, Y. sheng Hu, H. Li, X. Huang, L. Chen and L. Suo, *Angew. Chem., Int. Ed.*, 2021, **60**, 17547.
26 Q. Li, G. Liu, P. Kumar, F. Zhao, Y. Wang, T. Cai and Y. Chen, *Adv. Funct. Mater.*, 2025, **35**, 2416714.
27 L. Liu, Z. Shadike, N. Wang, Y. Chen, X. Cai, E. Hu and J. Zhang, *eScience*, 2024, **4**, 100268.
28 Y. Li, Y. Yang, Y. Lu, Q. Zhou, X. Qi, Q. Meng, X. Rong, L. Chen and Y. S. Hu, *ACS Energy Lett.*, 2020, **5**, 1156.

29 F. Wu, F. Chu, G. A. Ferrero, M. Sevilla, A. B. Fuertes, O. Borodin, Y. Yu and G. Yushin, *Nano Lett.*, 2020, **20**, 5391.
30 F. Chu, M. Wang, J. Liu, Z. Guan, H. Yu, B. Liu and F. Wu, *Adv. Funct. Mater.*, 2022, **32**, 2205393.
31 H. Ji, Z. Wang, Y. Sun, Y. Zhou, S. Li, J. Zhou, T. Qian and C. Yan, *Adv. Mater.*, 2023, **35**, 2208590.
32 X. Liu, Y. Ni, Z. Yang, Y. Lu, W. Xie, Z. Yan and J. Chen, *Adv. Energy Mater.*, 2025, **15**, 2403628.
33 N. S. Cattani, E. Noronha, J. Schmied, M. Frieges and H. Heimes, *Batteries*, 2024, **10**, 252.
34 M. Li, J. Yang, Y. Shi, Z. Chen, P. Bai, H. Su, P. Xiong, M. Cheng, J. Zhao and Y. Xu, *Adv. Mater.*, 2022, **34**, 2107226.
35 Q. Zhou, J. Ma, S. Dong, X. Li and G. Cui, *Adv. Mater.*, 2019, **31**, 1902029.
36 Y. Yamada and A. Yamada, *J. Electrochem. Soc.*, 2015, **162**, A2406.
37 O. Borodin, J. Self, K. A. Persson, C. Wang and K. Xu, *Joule*, 2020, **4**, 69.
38 Q. Zhao, X. Liu, S. Stalin, K. Khan and L. A. Archer, *Nat. Energy*, 2019, **4**, 365.
39 K. Mu, D. Wang, W. Dong, Q. Liu, Z. Song, W. Xu, P. Yao, Y. Chen, B. Yang, C. Li, L. Tian, C. Zhu and J. Xu, *Adv. Mater.*, 2023, **35**, 2304686.
40 H. Liu, S. Wang, W. Kong, Y. Liu, W. Ren and H. Wang, *Adv. Energy Mater.*, 2025, **15**, 2404046.
41 X. Yin, B. Li, H. Liu, B. Wen, J. Liu, M. Bai, Y. Zhang, Y. Zhao, X. Cui, Y. Su, G. Gao, S. Ding and W. Yu, *Joule*, 2025, **9**, 101823.
42 L. Wang, H. Shi, Y. Xie and Z. Wu, *Interdiscip. Mater.*, 2023, **2**, 789.
43 J. Pan, Y. T. Cheng and Y. Qi, *Phys. Rev. B:Condens. Matter Mater. Phys.*, 2015, **91**, 134116.
44 Y. Chen, F. Huo, S. Chen, W. Cai and S. Zhang, *Adv. Funct. Mater.*, 2021, **31**, 2102347.
45 H. Wu, Y. Xu, X. Ren, B. Liu, M. H. Engelhard, M. S. Ding, P. Z. El-Khoury, L. Zhang, Q. Li, K. Xu, C. Wang, J. G. Zhang and W. Xu, *Adv. Energy Mater.*, 2019, **9**, 1902108.
46 T. U. Wi, S. O. Park, S. J. Yeom, M. H. Kim, I. Kristanto, H. Wang, S. K. Kwak and H. W. Lee, *ACS Energy Lett.*, 2023, **8**, 2193.
47 J. Luo, J. Zhang, Z. Guo, Z. Liu, C. Wang and H. Jiang, *Adv. Mater.*, 2024, **36**, 2405956.
48 Q. Sun, S. Wang, Y. Ma, D. Song, H. Zhang, X. Shi and N. Zhang, *Adv. Mater.*, 2023, **35**, 2300998.
49 S. Zhang, Z. Li, Y. Zhang, X. Wang, P. Dong, S. Lei, W. Zeng, J. Wang, X. Liao, X. Chen, D. Li and S. Mu, *Energy Environ. Sci.*, 2025, **18**, 3807.
50 A. Maradesa, B. Py, J. Huang, Y. Lu, P. Iurilli, A. Mrozinski, H. M. Law, Y. Wang, Z. Wang, J. Li, S. Xu, Q. Meyer, J. Liu, C. Brivio, A. Gavrilyuk, K. Kobayashi, A. Bertei, N. J. Williams, C. Zhao, M. Danzer, M. Zic, P. Wu, V. Yrja, S. Pereverzyev, Y. Chen, S. V Kalinin, J. P. Schmidt, Y. Tsur, B. A. Boukamp, Q. Zhang, M. Gaberscek, R. O'Hayre and F. Ciucci, *Joule*, 2024, **8**, 1958.
51 Y. Lu, C. Zhao, J. Huang and Q. Zhang, *Joule*, 2022, **6**, 1172.
52 T. Yi, E. Zhao, Y. He, T. Liang and H. Wang, *eScience*, 2024, **4**, 100182.
53 J. Chen, Y. Peng, Y. Yin, Z. Fang, Y. Cao, Y. Wang, X. Dong and Y. Xia, *Angew. Chem., Int. Ed.*, 2021, **60**, 23858.